Eur. Phys. J. B **12**, 171–178 (1999)

THE EUROPEAN PHYSICAL JOURNAL B

EDP Sciences

Magnetic circular dichroism in lanthanide 4d-4f giant resonant photoemission: terbium

K. Starke[1,a], Z. Hu[1], F. Hübinger[1], E. Navas[1], G. Kaindl[1], and G. van der Laan[2]

[1] Institut für Experimentalphysik, Freie Universität Berlin, 14195 Berlin-Dahlem, Germany
[2] Daresbury Laboratory, Warrington WA4 4AD, UK

Received 23 February 1999

Abstract. Magnetic circular dichroism in lanthanide $4f$ photoemission (PE) multiplets was studied across the $4d$-$4f$ excitation threshold for the example of Tb metal. The combined experimental and theoretical analysis demonstrates that resonant enhancement of the $4f$ PE signal and large magnetic contrast in the PE intensity are obtained simultaneously, when the excitation energy is tuned to the absorption-edge maximum for parallel orientation of magnetization and circular-polarization light helicity.

PACS. 32.80.Dz Autoionization – 78.40.Kc Metals, semimetals, and alloys – 78.70.Dm X-ray absorption spectra

1 Introduction

Magnetic circular dichroism in X-ray absorption (XMCD) [1,2] has been widely used for element specific analyses of complex magnetic systems, such as garnets [3], spinels [4], multilayers [5–7], and alloys [8]. Most XMCD studies employ $3d$-transition metal (TM) $L_{2,3}$ edges and lanthanide $M_{4,5}$ edges, where a large change in absorption is obtained with circularly-polarized (CP) light excitation into the partially filled magnetic $3d$ or $4f$ shell when the sample magnetization is reversed. In favorable cases the absorption-edge intensity changes by more than 30%, corresponding to a large magnetic contrast which has been used for domain imaging [9,10]. Furthermore, element specific magnetic moments can be extracted from $L_{2,3}$ edge XMCD spectra of late TM with help of sum rules with an accuracy of $\sim$ 10% [11–13]. XMCD at lanthanide $M_{4,5}$ edges [3,14,15] can reveal the element-resolved magnetization in lanthanide-based alloys like TbFeCo, most relevant for magnetooptical storage.

Magnetic dichroism also exists in core-level photoemission (MDPE) [16,17] where it is not restricted to CP-light excitation but can similarly be obtained with linearly polarized light in chiral experimental geometries [18–20]. It is a unique merit of core-level photoemission that binding energies (BE) depend on the chemical environment of the emitting atom; they can shift by several eV from one compound to another [21]. These shifts are particularly well resolved in PE spectra of $4f$ lines which are intrinsically so narrow that even different atomic coordinations can be separated, such as surface and sub-surface layers (surface core-level shift) [22,23]. Recently, MDPE at lanthanide $4f$ lines with substantial core-level BE shifts was used to separate the magnetization of individual atomic layers at an interface [24].

$4f$-PE spectra of lanthanide elements generally consist of many multiplet lines between the Fermi level and some 15-eV BE [23]. As a typical example, the Tb $4f$-PE spectra [25,26] are shown in Figure 1a. They are obtained by CP light of 100-eV photon energy with photon momentum either (nearly) parallel or antiparallel to the remanent in-plane magnetization of the Tb-metal film. Upon magnetization reversal (or light helicity reversal), the relative Tb $4f$-multiplet intensities change strongly; this is also reflected in the associated intensity difference underneath (Fig. 1b), termed MCD spectrum [19].

Due to the localized nature of the $4f$ orbitals in heavy lanthanide atoms, $4f$-PE multiplets can be well described by atomic multiplet theory using electric dipole selection rules [27]. Starting from a ground-state f-electron configuration $4f^w$, with occupation number $w = 8$ for Tb, electric dipole excitation $E1$ of an f-electron into continuum states εl

$$4f^w(LS, J) \xrightarrow{E1} 4f^{w-1}(L''S'', J'') + \varepsilon l \qquad (1)$$

leaves the photoionized atom in the PE *final state* $4f^{w-1}$, with multiplet components labeled by their leading LS-coupling contributions $(L''S'', J'')$; for Tb the most intense ones are indicated in Figure 1b. Energy separations between the multiplet components scale with the intra-atomic $4f$-Coulomb interaction, usually parametrized by reduced Slater integrals to account for the screened f-hole in the PE final state [28]. A detailed agreement between experimental (for Tb in Fig. 1b) and theoretical MCD

[a] e-mail: starke@physik.fu-berlin.de

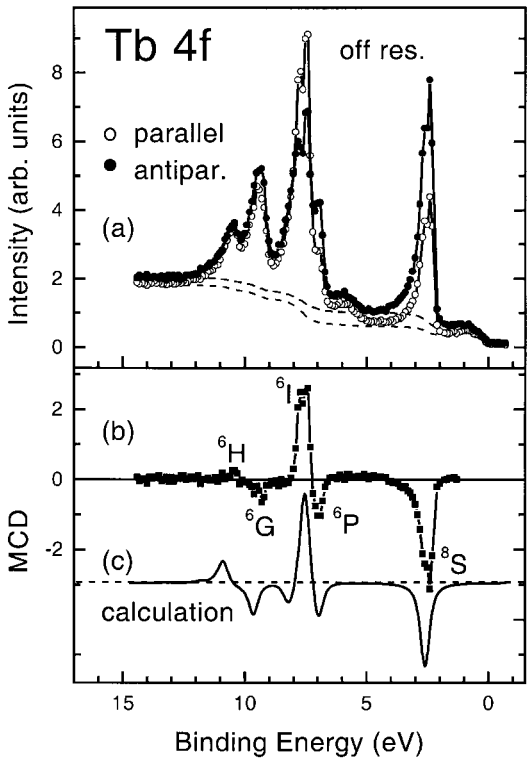

Fig. 1. (a) Off-resonance $4f$-PE spectra from a remanently magnetized Tb-metal film at 30 K, excited with CP light of $h\nu = 100$ eV, well below the $4d$-$4f$ excitation threshold. The relative intensities of the $4f$-multiplet components change upon reversal from "parallel" (open symbols) to "antiparallel" orientation (solid circles) between sample magnetization and photon helicity; from reference [26]. An integral background (dashed lines) has been subtracted before calculation of the difference (MCD) spectrum. (b) Difference spectrum of the experimental spectra in (a) compared with the calculated Tb-$4f$ MCD spectrum (c).

spectra (Fig. 1c) has been reached in all cases studied so far (also Gd [17] and Dy [29]), indicating that magnetic dichroism at the lanthanide $4f$ levels is suitably described by atomic multiplet theory. MDPE is expected to appear in the $4f$-PE spectra of *all* lanthanide elements provided that they exhibit phases with magnetically oriented f moments [30].

Aiming at an element selective analysis of compound systems we may exploit the fact that, for each final-state f-shell occupation number $w-1$, there is a characteristic $4f$-PE multiplet serving as a fingerprint of the associated lanthanide element [23,27]. However, except for a few favorite cases [31], the elemental $4f$-PE spectra overlap and it would be desirable to enhance selectively the $4f$-PE cross section of individual elements by resonant photoemission (RPE) [32–34]. In RPE, a particular photon energy $h\nu$ is chosen at which a *second* photoexcitation channel opens up that interferes constructively with the direct photoemission channel in equation (1). The cross-section enhancement is very effective at the $4d \rightarrow 4f$ giant resonance [35], where both shells involved are of the same principal quantum number and have a similar radial distribution. Although a coherent process, RPE is commonly described as a virtual two-step process [36]:

$$\begin{array}{ccc} 4f^w(LS,J) & \xrightarrow[a]{E1} & 4f^{w-1}+\varepsilon l \\ & \searrow^{b}_{E1} \quad \nearrow_{sCK} & \\ & 4d^9 4f^{w+1}(L'S',J') & \end{array} \qquad (2)$$

The same total final-state configuration ($4f^{w-1}\varepsilon l$) is reached via an "intermediate" $4d$-hole state, which decays through a radiationless super *Coster-Kronig* (sCK) Auger recombination. Magnetic circular dichroism in RPE was recently studied at the $3d \rightarrow 4f$ threshold ($M_{4,5}$ edge) of Gd [14] and Tb [37] where – at the associated high excitation energies of $h\nu \approx 1.2$ keV and above – the $E1$ transition along the indirect channel b is about four orders of magnitude stronger than channel a, so that resonant $4f$-PE spectra at $M_{4,5}$ are clearly dominated by the core excitation. By contrast, at the lanthanide $4d \rightarrow 4f$ threshold ($N_{4,5}$ edge), the $E1$ matrix elements for direct and indirect photoexcitation are of the same order of magnitude so that interference effects between both channels become important.

The influence of an indirect photoexcitation channel b on MDPE has so far only been studied for the case of Gd [38], which is a particularly simple case of a single (spin-orbit split) PE component due to the half-filled f shell in the ground state. In the present article we discuss a combined experimental and theoretical analysis of magnetic dichroism in RPE from lanthanides at the example of *terbium* metal, which is representative of the usually rich $4f$-PE multiplet structure of lanthanide elements.

2 Experimental

The experiments were performed at the beamline SX700-3 of the Berliner Elektronenspeicherring für Synchrotronstrahlung (BESSY). This bending-magnet beamline supplies a CP X-ray beam off the storage-ring plane with about 80% circularly polarized light (at a flux of $\sim 10^9$ photons/s/mrad/0.1‰ bandwidth) in the Tb $N_{4,5}$ energy region [39].

As samples we prepared (10 ± 1) nm thick Tb(0001) films epitaxially grown *in-situ* by metalvapor deposition on a W(110) single crystal [40]. A remanent nearly single-domain *in-plane* magnetization was achieved by Curie-point writing, *i.e.* the sample was heated above and subsequently cooled well below the highest ordering temperature ($T_N = 232$ K) inside the gap of an electromagnet (magnetic fields up to 0.2 tesla), placed inside the UHV chamber. XMCD spectra were recorded in the total-electron-yield (TEY) mode using a channeltron; PE spectra were obtained by a hemispherical energy analyzer, operated at 0.1-eV resolution. All photoelectrons from a wide cone (10°) about the Tb-surface normal were collected in order to minimize photoelectron-diffraction effects [41].

All XMCD and PE spectra were taken at 30 K sample temperature, *i.e.* close to complete ferromagnetic alignment of the Tb $4f$ moments. Recorded at an X-ray incidence angle of 30° with respect to the surface, all spectra have been corrected for saturation, assuming a ratio of 1 : 3 for the mean electron escape length over light-penetration depth within the standard procedure by Thole *et al.* [42].

For comparison XMCD spectra were also recorded with the electron analyzer in the constant-final-state (CFS) mode with a wide energy band pass (5 eV). The Tb $N_{4,5}$ spectral lines were reproduced, but with a three times larger pre-edge to giant-peak intensity ratio (Figs. 2 and 3) as compared to TEY detection. This effect is tentatively attributed to the different secondary-electron energy intervals used by the two detection modes; it should be considered when comparing XMCD-spectral regions of very different intensity with calculations.

3 Calculations

XMCD and RPE spectra were calculated in intermediate coupling using Cowan's relativistic Hartree-Fock (HF) code plus statistical exchange method [36]. Following the t-matrix approach [37] radiative transitions were considered to first order ($E1$) and the Coulomb interaction, responsible for the sCK decay, to infinite order. In the solid, intra-atomic correlation and relaxation can be included by scaling the HF value to typically 0.8. In previous studies of the Tb $M_{4,5}$ edge [37,43], the scaling parameters of the Slater integrals were found as $\kappa_1 = 0.84$, $\kappa_2 = 1$, and $\kappa_3 = 0.8$ for the ff Coulomb, df Coulomb, and df exchange interactions, respectively. In order to reproduce the experimental energy separation between the Tb $N_{4,5}$ giant resonance and the pre-edge peaks, it was essential to use $\kappa_3 = 0.7$. This indicates that the exchange interaction of the $4f$ shell with the $4d$ hole is better screened than that with the $3d$ hole, as it is expected for a shallower core level.

Use of the intermediate coupling scheme is mandatory, because in the photo-excited configuration $4d^9 4f^9$ the $4d$ spin-orbit (s.o.) interaction (2.5 eV) cannot be neglected compared to the Coulomb interaction (20 eV) [44]. However, the XA states can still be approximately labeled with the LS coupling scheme. A relatively small s.o. splits these states in separate J levels, whereas a larger s.o. will also mix different LS states for each particular J. Therefore, we will label the most pronounced spectral features according to their leading LSJ contribution. For the $4f$ RPE spectra the final-state lifetime was taken to be infinite, resulting in delta line forms which were convoluted by a Doniach-Sunjic line shape with $\Gamma = 0.17$ eV and asymmetry parameter $\alpha = 0.1$ and a Gaussian of $\sigma = 0.085$ eV to account for the intrinsic width and the instrumental broadening, respectively. We like to emphasize that the line widths in the calculated XA spectra resulted naturally from the sCK matrix elements and required no convolution [38].

4 Off-resonance 4f photoemission

At photon energies well below or above the $4d$-$4f$ excitation threshold, the indirect core-excitation channel can be neglected; direct photoexcitation Tb $4f^8 \rightarrow 4f^7 + \varepsilon l$ into the continuum εl shall be referred to as "off-resonance" PE. The many lines in the off-resonance Tb $4f$ PE spectrum in Figure 1 reflect the large number of $(L''S'', J'')$ multiplet components of the $4f^7$ final-state configuration [26,27,45]. The spectrum nicely separates into a high-spin ${}^8S_{7/2}$ line, at ~ 2.3 eV binding energy, and a group of low-spin lines ($S'' = 5/2$) above 7 eV, with the most intense lines labeled $({}^6I, \dots)$. The lowest-BE line ${}^8S_{7/2}$ corresponds to the Hund's-rule ground state of f^7, an S state with spherical f-charge distribution which yields the lowest final-state energy. The considerable energy spread of the f^7 multiplet over 10 eV reflects the substantial intra-atomic Coulomb interaction in the lanthanide $4f$-shell; it is smaller in the metallic solid as compared to an isolated Tb atom since $6s$ and $5d$ valence electrons screen the f hole in the PE final state.

For the off-resonance case, sum rules [46] have been formulated for MDPE, similar to those well known for XMCD (see above). The MDPE sum rules connect core-level multiplet component intensities in the limit of pure LS coupling with the ground-state orbital magnetic moment. However, to extract numbers from experimental $4f$ PE spectra, there are two main difficulties: (1) core-level PE-line intensities from crystalline solids are subject to photoelectron diffraction (PED) effects [41], which can alter the relative multiplet-component intensities, despite the non-angle resolved photoelectron detection used here (Sect. 2). (2) Although the MDPE sum rules are valid when integrating over the total $4f$-PE signal, they do not strictly apply to the separate LS terms since a proper description requires intermediate coupling (see above). However, according to the MDPE sum rule, we write the MCD-spectrum intensity of an individual L'' component [46]

$$I^1(L'') \propto [L(L+1) + l(l+1) - L''(L''+1)]\,\langle L_z \rangle, \quad (3)$$

with $L(l = 3)$ denoting the ground state (one-electron) orbital momentum. For the Tb ${}^7F(L = 3)$ ground state, equation (3) yields $I^1(L'') \propto [24 - L''(L''+1)]$, *i.e. negative* MCD for small $L'' \leq 4$ and *positive* MCD for large $L'' > 4$ (the spin S'' is irrelevant). This result agrees nicely with the experimental and theoretical (intermediate coupling) MCD spectra in Figures 1b and 1c: the strongest S, P, D, F, G lines ($L'' \leq 4$), labeled according to their dominant LS-contributions, are indeed negative in the MCD spectrum, whereas H and I lines ($L'' = 5, 6$) are positive.

5 XMCD spectra: identification of Tb $4d^9 4f^9$ intermediate states

Soon after discovery of the $N_{4,5}$ giant resonance in X-ray absorption [35], attempts were made to identify

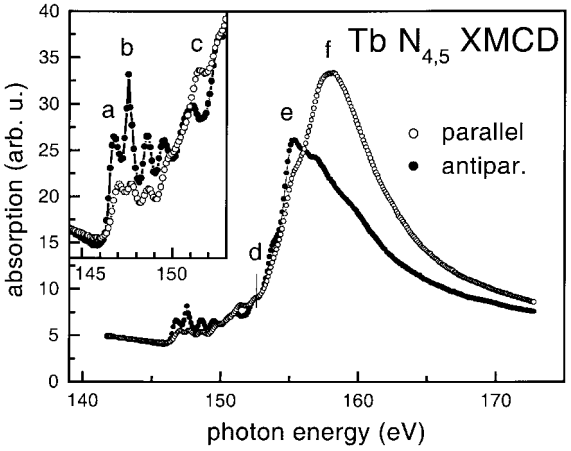

Fig. 2. X-ray absorption spectra of the Tb $4d \rightarrow 4f$ giant resonance ($N_{4,5}$ edge). The peak energy differs by ~ 3 eV between "parallel" (open symbols) and "antiparallel" orientation (solid circles) of magnetization and photon momentum. Inset: pre-edge peaks. Letters denote selected photon energies for resonant $4d$-$4f$ PE spectra in Figures 4, 5, and 6.

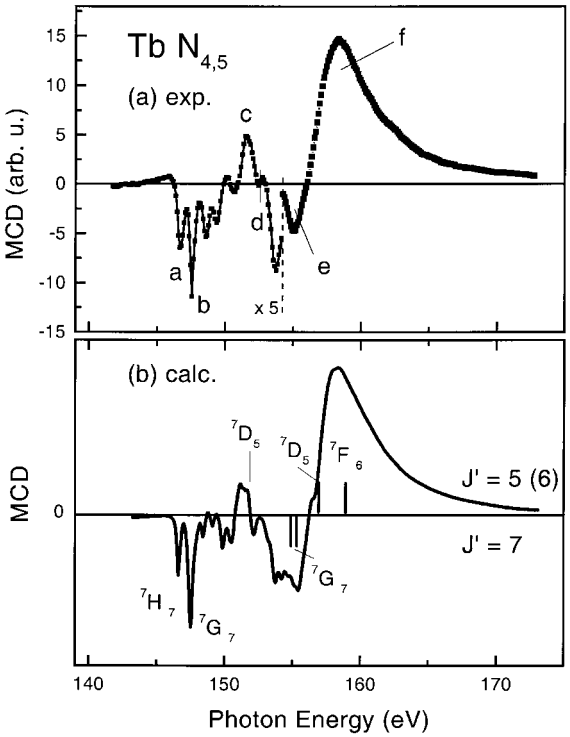

Fig. 3. (a) MCD spectrum calculated as difference of the experimental spectra in Figure 2. The weak pre-edge line intensity is 5× enlarged. (b) Calculated Tb XMCD spectrum including dominant LS-coupling characters of the most intense lines. Note that $4d$-hole states of high (low) J' appear as negative (positive) features in the MCD spectrum.

the observed spectral lines [47]. Recently, calculations by Ogasawara and Kotani [48] have been cited in comparison with experimental lanthanide $N_{4,5}$ XMCD spectra by Muto *et al.* [49]; but so far no identification of the Tb $4d^9 4f^9$ multiplet lines has been attempted.

High-resolution Tb-$N_{4,5}$ XMCD spectra are presented in Figure 2. For both orientations of photon momentum and Tb magnetization, the spectra are dominated by an asymmetrically broadened giant resonance line. The absorption maxima are located at different energies: at ~ 155 eV for antiparallel and at ~ 158 eV for parallel orientation. The inset magnifies a group of much weaker pre-edge lines starting at ~ 147 eV. They correspond to low-energy states of the Tb $4d^9 4f^9$ multiplet which is spread over 10 eV by the strong Coulomb correlation between $4d$ and $4f$ electrons. The large $4d$-$4f$ overlap also results in a considerable width of the giant-resonance lines of about 9 eV, due to the rapid super Coster-Kronig (sCK) decay within a few 10^{-17} s. Hence, at the giant resonance, the intermediate $4d$-hole state decays on the same time scale as is generally stated for the photoexcitation process [50]. By contrast, the much narrower pre-edge lines (see inset of Fig. 2) show lifetime widths of typically $2\Gamma \approx 0.4$ eV which correspond to much longer $4d$-hole life times on the order of 10^{-15} s.

The corresponding MCD spectrum, *i.e.* the difference between "parallel" and "antiparallel" spectra, is shown in Figure 3a, along with the theoretical spectrum in Figure 3b calculated in intermediate coupling. Note that in the limit of vanishing $4d$ spin-orbit coupling, the Tb-XA spectra would simply contain ^7D, ^7F, and ^7G states, which are reached *via* $E1$ from the $4f^8$ ($^7F_6$) ground state without violation of the LS-coupling selection rules $\Delta L = -1, 0, +1$ and $\Delta S = 0$. Although $4d$ s.o. coupling weakens the LS rules and allows for, *e.g.*, ^7H pre-edge states, corresponding to $\Delta L = +2$, the "LS-allowed" transitions are still the most intense ones giving rise to the giant resonance (thick vertical bars in Fig. 3b).

The good signal-to-noise ratio and the high energy resolution of the experimental MCD spectrum (about 4 times better than the smallest intrinsic width of 0.4 eV) allow a detailed comparison. It shows that intermediate $4d$-hole states with dominant angular momentum $J' = 7$ become visible as MCD *minima*, while those with $J' = 5$ and – less pronounced – with $J' = 6$ lead to *maxima*; *i.e.*, J' can in part be read from the sign of the MCD signal. This property of MCD spectra is just a consequence of the fact that $E1$ transitions with CP light between core levels with an unequal magnetic M-sublevel population preferentially follow $\Delta J = -\Delta M$ [38,51].

This $\Delta J = -\Delta M$ preference is formally understood as follows: s.o. coupling leaves $\Delta J = 0, \pm 1$ as strict selection rule which directly connects the initial state with the *total* final state $|J'M'\rangle$ describing the $4d^9 4f^9$ excitation state (X-ray absorption state). Angular and radial part of the $E1$ transition probabilities $\sigma_q^{JJ'}$ for different photon polarizations, $q = +1, 0$, and -1, are conveniently separated by help of the Wigner-Eckart theorem [36]

$$\boldsymbol{\sigma}_q^{JJ'} = |\langle J'M'|\mathbf{P}_q|JM\rangle|^2 = \underbrace{|\langle J'\|\mathbf{P}\|J\rangle|^2}_{\mathbf{S}_{JJ'}} \begin{pmatrix} J & 1 & J' \\ -M & q & M' \end{pmatrix}^2 . \quad (4)$$

The $3j$-symbol (in parenthesis) describes the coupling of photon and ground-state angular momentum J in a compact way. It vanishes unless $q = M - M' = -\Delta M$. Most importantly, it gives very different weights of the line strengths $\mathbf{S}_{JJ'}$ for opposite helicities: in $\Delta M = -1$ transitions, from the Tb $4f^8(^7F_6)$ ground state $|J = 6, M = -6\rangle$ (fully magnetized) to $M' = -7$, only $J' = 7$ is an allowed final state, *i.e.* $\Delta J = -\Delta M$ holds strictly. In $\Delta M = +1$ transitions to $M' = -5$, the $J' = 5$ final state ($\Delta J = -\Delta M$) dominates by far; $J' = 6$ contributes only $\sim 14\%$, and $J' = 7$ can be almost neglected ($\sim 1\%$).

The detailed agreement between experimental and calculated MCD spectra in Figure 3 is striking, and the intermediate-coupling calculation confirms the J' assignments obtained from the sign of the XMCD spectrum. Having achieved a consistent description of the $E1$-excitation step along the indirect channel b, we now proceed to the $4d \rightarrow 4f$ PE resonance process as a whole.

6 Resonant 4f photoemission

For photoexcitation energies near the $N_{4,5}$ threshold, the indirect $4d$-$4f$ core-excitation channel is up to one order larger than the direct channel [44]. Concerning MDPE, we anticipate that the involvement of the inner shell will change the relative intensities of the Tb $4f$ multiplet components. Off-resonance, there was no other restriction on the total momentum in the final state J' than the $\Delta J = -\Delta M$ preference (see above). In resonant $4d \rightarrow 4f$ PE, when the photon energy is tuned to a narrow $N_{4,5}$ absorption line associated with a $4d^9 4f^8$ state of sufficiently pure J' character, we expect an interference of direct and indirect excitation channels only for this specific J' [38].

Experimental resonant $4f$ PE spectra are presented in Figure 4 for selected photoexcitation energies $a, b, \ldots f$ across the $4d$-$4f$ threshold, as indicated in Figures 2 and 3a. The associated experimental MCD spectra are given in Figure 5, together with calculated MCD spectra (dashed lines). At energies a and b, the antiparallel dominates over the parallel spectrum at all multiplet lines. This is most pronounced at energy b which corresponds to an intermediate state of high $^7G_{J'=7}$ purity; thus it is reached from the $J = 6$ ground state by $\Delta M = -1$ (antiparallel) transitions. Absorption structure a is less pure comprising $J' = 6$ and 7 states. Unlike off-resonance (Fig. 1b), the MCD spectra at a and b are clearly *negative* over the whole $4f$-PE multiplet (Fig. 5). Furthermore, the low-BE $^8S_{7/2}$ component becomes the most intense line of the antiparallel spectrum, see Figure 4.

At pre-edge energy c, the high-L'' lines ^6G, ^6H, and ^6I of the parallel spectrum clearly dominate, corresponding to an overall *positive* MCD spectrum (except the small negative $^8S_{7/2}$ component). In addition there is considerable multiplet intensity at binding energies above 12 eV (dashed vertical line in Fig. 4) where no spectral weight is discernible neither at a and b, nor off-resonance, *cf.* Figure 1. The many weak Tb $4f$-PE lines between $\sim$ 12 eV and $\sim$ 15 eV binding energy are assigned to "spin-flip" $S'' = 3/2$ states ($^4L''$). Starting from the Tb

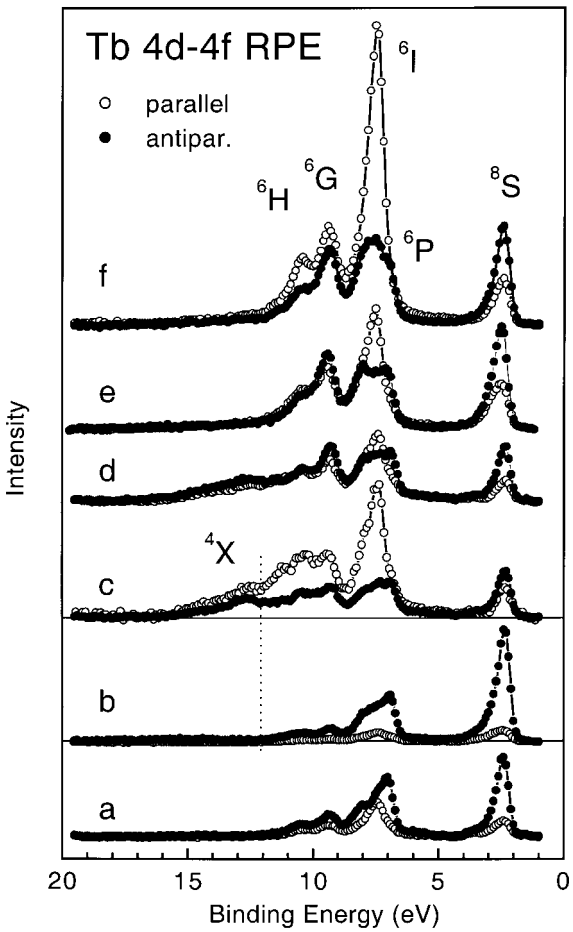

Fig. 4. Resonant $4f$-MDPE spectra at excitation energies given in Figure 2 (Fig. 3). An integral background (like in Fig. 1a) has been subtracted. Spin-flip PE final states ^4X (X: various L'' values) appear above 12 eV binding energy (dashed line).

$4f^8\ ^7F(S = 3)$ ground state, such a spin-flip is forbidden off resonance, according to the restrictive LS-coupling rule $\Delta S = 0$, which is approximately valid for the direct photoexcitation channel involving only the $4f$ shell and the continuum where s.o. interaction is weak and negligible, respectively; yet in RPE spin flips become allowed through $4d$-s.o. coupling. The higher BE (> 12 eV) of the spin-flip lines visualizes the exchange energy of some 5 eV which is needed to "flip" one f-spin in the $4f^7$ configuration, *i.e.* to go from $\uparrow\uparrow\uparrow\uparrow\uparrow\uparrow\downarrow$ (^6I line) to $\uparrow\uparrow\uparrow\uparrow\uparrow\downarrow\downarrow$. The calculation shows low-spin states ($^5L'$) of the $4d^9 4f^9$ configuration at energy position c in the absorption spectrum; the energy difference of 4.9 eV between pre-edge structures c and a reflects the $4d$-$4f$ exchange energy.

At energy d, which is a point of vanishing MCD in the absorption spectrum (Fig. 3), the MCD spectrum Figure 5d yields the same signs as off-resonance (Fig. 1b). The corresponding PE spectra in Figure 4d also indicate a non-vanishing spin-flip probability.

Most important for applications are the giant-resonance maxima e and f where the cross-section enhancement

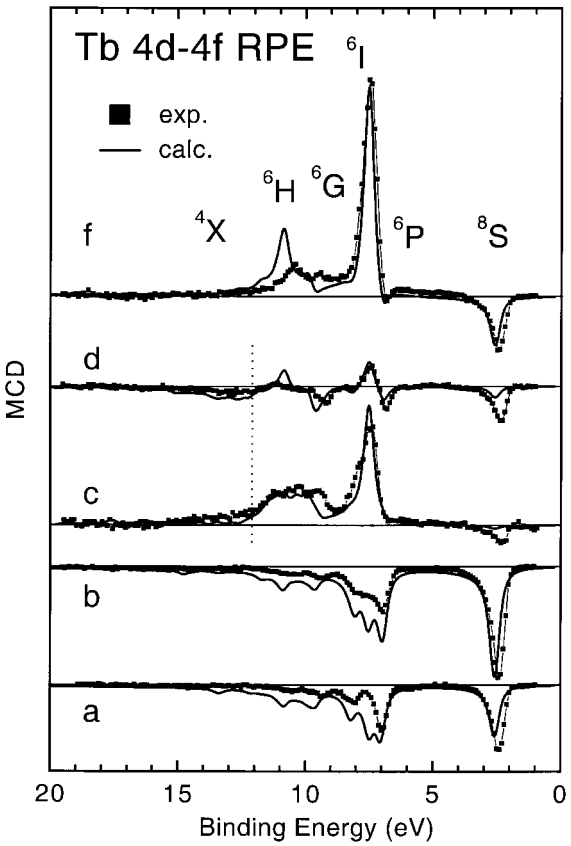

Fig. 5. Experimental MCD spectra (squares) obtained from the spectra in Figure 4, compared with theoretical MCD spectra (solid curves) calculated in intermediate coupling. Spin-flip PE final states ^4X (X: various L'' values) appear above 12 eV binding energy (dashed line).

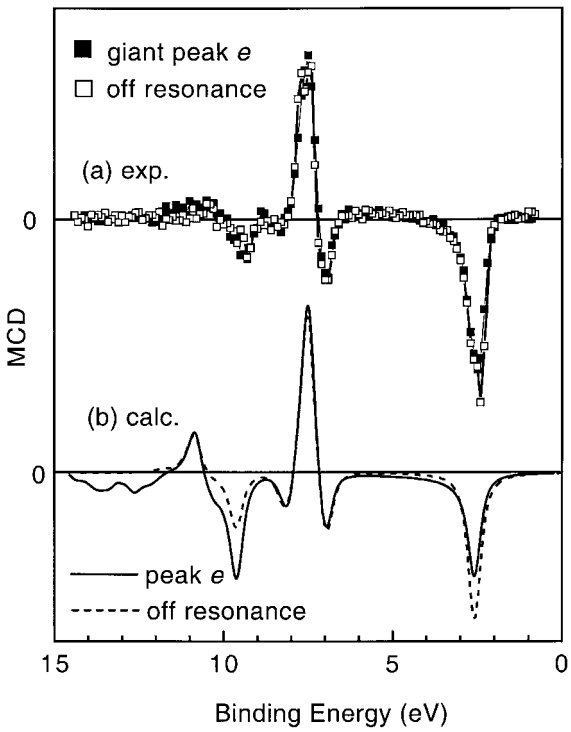

Fig. 6. Comparison of (a) experimental MCD spectra of the resonant (solid symbols) and off resonant (open symbols) Tb $4f$-PE multiplet; (b) corresponding calculated MCD spectra.

is strongest. At the giant antiparallel peak e, the $4f$-RPE spectra in Figure 4e closely resemble the off-resonance spectra (Fig. 1a). A detailed comparison of the experimental MCD spectra in Figure 6a shows that they are indeed nearly identical: matched in intensity at the ^6I line, resonant and off-resonant MCD multiplet intensities follow each other closely. The resonant ^8S MCD is found to be slightly less negative at e than off resonance (Fig. 6a); this trend is also reproduced (but larger) in the calculation (Fig. 6b). At high binding energies, near 9.5 eV (^6G) and above 12 eV, the calculation expects more spectral intensity. This discrepancy exists already for the off-resonance case, see Figure 1b. It is tentatively attributed to configuration interaction (CI) [37] involving the Tb $5p$ shell which is close in energy to the high-BE $4f$ components; CI is not included in the present calculation, but can in principle change the relative intensities within a PE multiplet [52].

The observed similarity between resonant and off-resonant spectra indicates that at the giant-resonance energy e the J'-selection is not very stringent. This can be understood as a consequence of the large Lorentzian width of the giant-resonance lines of $2\Gamma \approx 9$ eV (*viz.* Fig. 2) causing a large overlap between the broad absorption lines, $^7G_7$, $^7D_5$, and $^7F_6$, in the giant-resonance peak region; see Figures 2 and 3. Since they carry all three possible J' characters, there can be no strict J' selection as it is found, by contrast, at the sharp pre-edge line b.

At the giant peak for parallel orientation (f) the $4f$-PE cross section enhancement is largest and the dichroic effect is strong, particularly at the ^6I PE line (Figs. 4f and 5f) [26]. Agreement between experimental and calculated MCD spectra is excellent for all low-BE components (^8S, ^6P, ^6I), while high-BE component intensities are overestimated in the calculation (see above). The resonantly enhanced ^8S and ^6I PE lines yield MCD signals of opposite sign. This is potentially useful for domain-imaging by photoelectron-emission microscopes (PEEM): the two very intense PE lines yield reversed magnetic contrast and are separated by only ~ 5 eV, corresponding to only a few percent of the photoelectron kinetic energy.

7 Summary and conclusions

We have studied magnetic circular dichroism at Tb $4f$ levels in resonant photoemission at the $4d \rightarrow 4f$ excitation threshold. Comparison with an intermediate-coupling multiplet calculation yields a detailed understanding of the experimental XMCD and resonant MDPE spectra. In particular, largely different Tb $N_{4,5}$-edge absorption spectra are obtained from oppositely magnetized samples when CP soft X-rays are used, including an apparent 3-eV shift in the giant resonance maximum. The high XMCD

contrast could be used to monitor the degree of circular polarization of soft X-ray beamlines in the 150-eV range.

Already in 1993, MDPE at the $4d \rightarrow 4f$ threshold was used in a first successful study of magnetic surface domains of Gd/Fe and Tb/Fe systems [53]. Yet, conducted at a bending-magnet beamline, CP X-rays could be obtained only at reduced photon flux, and the observed magnetic contrast was weak.

The potential of future photoelectron-emission microscope (PEEM) experiments may be estimated on the basis of recent data obtained by Bauer and coworkers from Pb on W(110) [54,55]. There, images were recorded at the BESSY-1 undulator beamline TGM5, using Pb-5d photoelectrons excited at $h\nu \approx 60$ eV with an experimental core-level line width of 0.5 eV (at about 4×10^{16} photons/s/cm^2 [55]). This photon energy was chosen because of the extremely large Pb 5d-PE cross section of several 10 Mb (~ 60 Mb according to Ref. [56]). Earlier detailed analyses of Gd and other RE elements by Richter *et al.* [57] yield a similar size for the $4f$ PE-cross section at the $4d$-$4f$ giant resonance maximum (~ 30 Mb). According to the projected figures of UE56/1 at BESSY-2, an undulator beamline at a 3rd-generation synchrotron source will allow to illuminate samples with $\sim 10^{16}$ photons/s/cm^2 at very small bandwidths of ~ 50 meV. This is well below the $4f$-PE line surface core-level shift of RE metals [23], so that even small chemical shifts appearing, *e.g.*, at RE interfaces [24], can be resolved.

The present analysis has demonstrated that high magnetic contrast can be obtained at the resonantly enhanced high-spin (^8S) and low-spin (^6I) Tb $4f$-PE lines. These PE lines are suggested as a valuable tool in chemically specific magnetic-domain imaging by PEEM at high-brilliance synchrotron-radiation facilities, where use of photoelectron signals with energy discrimination [54,58] may open the door to exploit core-level BE shifts for imaging.

This work is supported by the Bundesminister für Bildung, Wissenschaft, Forschung und Technologie (BMBF), project No. 05-SC5 KEB-6.

References

1. G. Schütz, W. Wagner, W. Wilhelm, P. Kienle, R. Zeller, R. Frahm, G. Materlik, Phys. Rev. Lett. **58**, 737 (1987); C.T. Chen, F. Sette, Y. Ma, S. Modesti, Phys. Rev. B **42**, 7262 (1990).
2. For a recent review see: J. Stöhr, R. Nakajima, IBM J. Res. Develop. **42**, 73 (1998).
3. P. Rudolf, F. Sette, L.H. Tjeng, G. Meigs, C.T. Chen, J. Magn. Magn. Mater. **109**, 109 (1992).
4. G. van der Laan, C.M.B. Henderson, R.A.D. Pattrick, S.S. Dhesi, P.F. Schofield, E. Dudzik, D.J. Vaughan, Phys. Rev. B **59**, 4314 (1999).
5. Y. Wu, J. Stöhr, B.D. Hermsmeier, M.G. Samant, D. Weller, Phys. Rev. Lett. **69**, 2307 (1992).
6. Y.U. Idzerda, L.H. Tjeng, H.-J. Lin, C.J. Gutierrez, G. Meigs, C.T. Chen, Phys. Rev. B **48**, 4144 (1993).
7. C.T. Chen, Y.U. Idzerda, H.-J. Lin, G. Meigs, A. Chaiken, G.A. Prinz, G.H. Ho, Phys. Rev. B **48**, 642 (1993).
8. S. Pizzini, A. Fontaine, E. Dartyge, C. Giorgetti, F. Baudelet, J.P. Kappler, P. Boher, F. Giron, Phys. Rev. B **50**, 3779 (1994).
9. J. Stöhr, Y. Wu, B.D. Hermsmeier, M.G. Samant, G.R. Harp, S. Koranda, D. Dunham, B.P. Tonner, Science **259**, 658 (1993).
10. P. Fischer, G. Schütz, G. Schmahl, P. Guttmann, D. Raasch, Z. Phys. B **101**, 313 (1997).
11. P. Carra, B.T. Thole, M. Altarelli, X. Wang, Phys. Rev. Lett. **70**, 694 (1993).
12. B.T. Thole, P. Carra, F. Sette, G. van der Laan, Phys. Rev. Lett. **68**, 1943 (1992).
13. C.T. Chen, Y.U. Idzerda, H.-J. Lin, N.V. Smith, G. Meigs, E. Chaban, G.H. Ho, E. Pellegrin, F. Sette, Phys. Rev. Lett. **75**, 152 (1995).
14. Z. Hu, K. Starke, G. van der Laan, E. Navas, A. Bauer, E. Weschke, C. Schüßler-Langeheine, E. Arenholz, A. Mühlig, G. Kaindl, J.B. Goedkoop, N.B. Brookes, Phys. Rev. B **59**, 9737 (1999).
15. C. Bordel, S. Pizzini, J. Vogel, K. Mackay, J. Voiron, R.M. Galéra, A. Fontaine, P. Auric, J.B. Goedkoop, N.B. Brookes, Phys. Rev. B **56**, 8149 (1997); J. Schillé, P. Sainctavit, C. Cartier, C. Brouder, J.P. Kappler, G. Krill, Solid St. Commun. **85**, 787 (1993).
16. L. Baumgarten, C.M. Schneider, H. Petersen, F. Schäfers, J. Kirschner, Phys. Rev. Lett. **65**, 492 (1990).
17. K. Starke, E. Navas, L. Baumgarten, G. Kaindl, Phys. Rev. B **48**, 1329 (1993).
18. Ch. Roth, F.U. Hillebrecht, H.B. Rose, E. Kisker, Phys. Rev. Lett. **70**, 3479 (1993).
19. B.T. Thole, G. van der Laan, Phys. Rev. B **49**, 9613 (1994); G. van der Laan, Phys. Rev. B **51**, 240 (1995).
20. R. Feder, J. Henk, in *Spin-Orbit Influenced Spectroscopies of Magnetic Solids*, edited by H. Ebert, G. Schütz (Springer, Berlin, 1996).
21. K. Siegbahn, C. Nordling, G. Johansson, J. Hedman, P.F. Hedén, K. Hamrin, U. Gelius, T. Bergmark, L.O. Werme, R. Manne, Y. Baer, *ESCA Applied to Free Molecules* (North Holland, Amsterdam, 1969).
22. P.H. Citrin, G.K. Wertheim, Y. Baer, Phys. Rev. Lett. **41**, 1425 (1978).
23. G. Kaindl, A. Höhr, E. Weschke, S. Vandré, C. Schüßler-Langeheine, C. Laubschat, Phys. Rev. B **51**, 7920 (1995).
24. E. Arenholz, K. Starke, G. Kaindl, Appl. Phys. Lett. **71**, 3430 (1997).
25. E. Navas, K. Starke, C. Laubschat, E. Weschke, G. Kaindl, Phys. Rev. B **48**, 14754 (1993).
26. K. Starke, L. Baumgarten, E. Arenholz, E. Navas, G. Kaindl, Phys. Rev. B **50**, 1317 (1994).
27. P.A. Cox, J.K. Lang, Y. Baer, J. Phys. F **11**, 113 (1981).
28. B. Johansson, N. Mårtensson, Phys. Rev. B **21**, 4427 (1980).
29. E. Arenholz, E. Navas, K. Starke, L. Baumgarten, G. Kaindl, Phys. Rev. B **51**, 8211 (1995).
30. B.T. Thole, G. van der Laan, Phys. Rev. Lett. **70**, 2499 (1993).
31. E. Arenholz, K. Starke, G. Kaindl, P.J. Jensen, Phys. Rev. Lett. **80**, 2221 (1998).
32. W. Lenth, F. Lutz, J. Barth, G. Kalkoffen, C. Kunz, Phys. Rev. Lett. **41**, 1185 (1978).

33. J.W. Allen, L.I. Johansson, R.S. Bauer, I. Lindau, S.B.M. Hagström, Phys. Rev. Lett. **41**, 1499 (1978).
34. W. Gudat, S.F. Alvarado, M. Campagna, Solid St. Commun. **28**, 943 (1978).
35. T.M. Zimkina, V.A. Fomichev, S.A. Gribovskii, J.J. Zhukova, Sov. Phys. Solid State **9**, 1128 (1967).
36. R.D. Cowan, *The Theory of Atomic Structure and Spectra* (University of California Press, Berkeley, 1981).
37. G. van der Laan, E. Arenholz, Z. Hu, A. Bauer, E. Weschke, C. Schüßler-Langeheine, E. Navas, A. Mühlig, G. Kaindl, J.B. Goedkoop, N.B. Brookes, Phys. Rev. B **59**, 8835 (1999).
38. K. Starke, E. Navas, E. Arenholz, Z. Hu, L. Baumgarten, G. van der Laan, C.T. Chen, G. Kaindl, Phys. Rev. B **55**, 2672 (1997).
39. H. Petersen, M. Willmann, F. Schäfers, W. Gudat, Nucl. Instrum. Methods Phys. Res. Sect. A **333**, 594 (1993).
40. J. Kolaczkiewicz, E. Bauer, Surf. Sci. **175**, 487 (1986).
41. B. Hermsmeier, J. Osterwalder, D.J. Friedman, B. Sincovic, T. Tran, C.S. Fadley, Phys. Rev. B **42**, 11895 (1990).
42. B.T. Thole, G. van der Laan, J.C. Fuggle, G.A. Sawatzky, R.C. Karnatak, J.-M. Esteva, Phys. Rev. B **32**, 5107 (1985).
43. G. van der Laan, B.T. Thole, G.A. Sawatzky, J.B. Goedkoop, J.C. Fuggle, J.M. Esteva, R.C. Karnatak, J.P. Remeika, H.A. Dabkowska, Phys. Rev. B **34**, 6529 (1986).
44. The atomic Hartree-Fock values of the Slater integrals and spin-orbit parameters for the photoabsorption state $4d^9\ 4f^9$ are $F^2(ff) = 15.067$, $F^4(ff) = 9.461$, $F^6(ff) = 6.809$, $\zeta(4f) = 0.225$, $\zeta(4d) = 2.383$, $F^2(df) = 16.841$, $F^4(df) = 10.767$, $G^1(df) = 19.846$, $G^3(df) = 12.477$, $G^5(df) = 8.827$ eV. Those for the initial state and photoemission final state are given in reference [43]. The Coster-Kronig matrix elements are:

$$\begin{aligned} R^0(4d,4f;4f,\varepsilon s) &= -0.2824\,\text{eV}/\sqrt{Ry};\\ R^{0,2,4}(4d,4f;4f,\varepsilon d) &= -0.0133, 0.0323,\\ &\quad 0.0448\,\text{eV}/\sqrt{Ry};\\ R^{0,2,4}(4d,4f;4f,\varepsilon g) &= -3.3744, -1.9316,\\ &\quad -1.3039\,\text{eV}/\sqrt{Ry};\\ R^{0,2}(4d,4f;4f,\varepsilon i) &= -0.26695, -0.14385\,\text{eV}/\sqrt{Ry}. \end{aligned}$$

The dipole matrix elements are:

$$\begin{aligned} \langle 4d\|r\|4f\rangle &= 1.08979\,\text{a.u.};\\ \langle 4f\|r\|\varepsilon d\rangle &= 0.03620\,\text{a.u.}/\sqrt{Ry};\\ \langle 4f\|r\|\varepsilon g\rangle &= -0.34293\,\text{a.u.}/\sqrt{Ry}. \end{aligned}$$

45. F. Gerken, A.S. Flodström, J. Barth, L.I. Johansson, C. Kunz, Phys. Scripta **32**, 43 (1985).
46. G. van der Laan, B.T. Thole, Phys. Rev. B **48**, 210 (1993).
47. J. Sugar, Phys. Rev. B **5**, 1785 (1972).
48. H. Ogasawara, A. Kotani, J. Phys. Soc. Jap. **64**, 1394 (1995).
49. S. Muto, S.-Y. Park, S. Imada, K. Yamaguchi, Y. Kagoshima, T. Miyahara, J. Phys. Soc. Jap. **63**, 1179 (1994).
50. J.W. Gadzuk, *in Photoemission from Surfaces*, edited by B. Feuerbacher, B. Fitton, R.F. Willis (Wiley and Sons, New York, 1977), Chap. 7.
51. J.B. Goedkoop, B.T. Thole, G. van der Laan, G.A. Sawatzky, F.M.F. de Groot, J.C. Fuggle, Phys. Rev. B **37**, 2086 (1988).
52. G. van der Laan, M. Surman, M.A. Hoyland, C.F.J. Flipse, B.T. Thole, H. Ogasavara, Y. Seino, A. Kotani, Phys. Rev. B **46**, 9336 (1992).
53. T. Kachel, W. Gudat, K. Holldack, Appl. Phys. Lett. **64**, 655 (1994).
54. E. Bauer, C. Koziol, G. Lilienkamp, T. Schmidt, J. Electron Spectrosc. Relat. Phenom. **84**, 201 (1997).
55. T. Schmidt, S. Heun, J. Slezak, J. Diaz, K.C. Prince, G. Lilienkamp, E. Bauer, Surf. Rev. Lett. **5**, 1287 (1998).
56. J.J. Yeh, I. Lindau, At. Data Nucl. Data Tables **32**, 1 (1985).
57. M. Richter, M. Meyer, M. Pahler, T. Prescher, E. von Raven, B. Sonntag, H.-E. Wetzel, Phys. Rev. A **40**, 7007 (1989).
58. J. Stöhr, H.A. Padmore, S. Anders, T. Stammler, M.R. Scheinfein, Surf. Rev. Lett. **5**, 1297 (1998).